Composites Part C: Open Access 13 (2024) 100432

Contents lists available at ScienceDirect

Composites Part C: Open Access

journal homepage: www.elsevier.com/locate/composites-part-c-open-access

Optimum design method for structural configuration and fiber arrangement for fiber-reinforced composites

Yusuke Fujimoto [a], Kozo Furuta [b,*], Tsuguo Kondoh [a], Hao Li [b], Kazuhiro Izui [b], Shinji Nishiwaki [a]

[a] Department of Mechanical Engineering and Science, Kyoto University, 615-8540, Kyoto, Japan
[b] Department of Micro Engineering, Kyoto University, 615-8540, Kyoto, Japan

ARTICLE INFO

Keywords:
Fiber reinforced composites
Mean compliance minimization
Topology optimization
Level-set method
Orientation optimization
Direction tensor
Streamline control

ABSTRACT

Fiber-reinforced composite materials, exemplified by CFRP, offer the possibility of achieving lightweight, high-stiffness, and high-strength structures by continuously and evenly distributing fibers. While topology and orientation optimization methods have been developed for anisotropic materials in the past, there remains a gap in design methods that consider manufacturability, especially for continuous fiber materials. In this study, we propose a design method that takes into account manufacturability, focusing on the aspects of continuity and uniformity in fiber-reinforced composite optimum design. Specifically, we introduce a two-stage optimization approach. In the first stage, we conduct concurrent optimization of topology and fiber orientation. We utilize a level-set function to represent topological configuration, while for orientation, we introduce a "double angle vector", which enables us to consider fiber properties such as angular periodicity. These design variables are updated by solving partial differential equations based on reaction–diffusion equations. In the second stage, leveraging the optimal orientations obtained in the first stage, we optimize the path-line generation for the manufacture of continuous fiber materials. We introduce a scalar function representing path lines and formulate an optimization problem to ensure that the path lines are both evenly spaced and continuous. The update of design variables in this state is also achieved via solving the partial differential equation. Through the development of this two-stage optimization method, we aim to create an optimal structure with manufacturable continuous fiber materials, incorporating both the topology and fiber orientation that satisfy the requirements of continuity and uniformity.

1. Introduction

The material properties significantly influence the performance of a mechanical product. In other words, intensifying the material properties improves the product's overall performance. Developing new artificial materials is an appealing strategy for enhancing the performance of mechanical products, as natural materials like steel have limitations in terms of rigidity, weight, and other properties. Fiber-reinforced composites, exemplified by Carbon Fiber-Reinforced Plastics (CFRP), consist of a structure in which reinforcing fibers are embedded within the matrix material. They have found extensive applications, ranging from everyday essentials to heavy machinery products, serving as a viable alternative to metals due to their lightweight, high strength, and rigidity when subjected to loads in the direction of the fibers.

However, fiber-reinforced composites exhibit orthotropic material properties, implying that they possess exceptional strength and stiffness along the fiber direction but relatively low properties in the direction perpendicular to the fibers. Consequently, when designing and manufacturing products, it is imperative to consider the orientation of the fibers. For instance, components produced through injection molding are layered to create parts with pseudo-isotropic properties. This method offers advantages in terms of manufacturing cost, ease of fabrication, and avoidance of stiffness reduction in specific directions [1]. Despite these advantages, this laminating approach introduces a misalignment between the fiber orientation and principal stress directions. Furthermore, composites manufactured via injection molding incorporate discontinuous short fibers and particle structures, which are cost-effective and easy to process but exhibit relatively lower stiffness and strength when compared to continuous-fiber composites [2,3]. Manufacturing methods that continuously arrange fibers in a controlled manner, such as Automated Fiber Placement (AFP) [4] or Tailored Fiber Placement (TFP) [5], have been developed to address these challenges and enable the design of higher-performance products. The fibers manufactured by these methods are required to be distributed continuously and evenly. In this paper, we focus on constructing an

* Corresponding author.
E-mail address: furuta.kozo.5n@kyoto-u.ac.jp (K. Furuta).

https://doi.org/10.1016/j.jcomc.2024.100432
Received 30 October 2023; Received in revised form 24 December 2023; Accepted 5 January 2024
Available online 13 January 2024

optimum design method for the structural configuration and fiber arrangement for continuous fibers fabricated by TFP.

As has been discussed above, the orthotropic design of continuous-fiber composite materials is promising to improve the mechanical performance of various industrial products. Therefore, the capability to predict the structural response of fiber composites can significantly benefit from design and optimization. However, to date, most designs are still limited to rather simple structures, which impede the full exploitation of continuous-fiber composite materials. In stark contrast to empirical designs, structural optimization is a powerful numerical method combining mathematical and physical rationale with simulations to deliver innovative structures that can maximize functional performances. One of the most effective design methods for structures composed of continuous-fiber composites is the simultaneous optimization of topology and orientation of anisotropic elastic materials. This allows us to combine the advantages of topology optimization [6], known to have a very high degree of design freedom, with fiber orientation optimization. In terms of practical use, one plausible approach involves generating the structure through topology optimization and subsequently utilizing trajectory software to design the orientation of continuous fibers. Conversely, concurrent optimization of structural configuration and fiber arrangement enables more enhanced product designs by considering the mutual influence between the structure and angles during the optimization process, thus potentially leading to higher performance.

Continuous Fiber Angle Optimization (CFAO) [7–9] is an approach utilized for designing fiber arrangements, involving continuous updates of the orientation angles. However, these methods tend to demonstrate a strong dependency on initial angle values, which presents obstacles to their integration with topology optimization; thus Stegmann and Lund developed the discrete material optimization method as an alternative approach [10]. Zhou et al.. constructed the multi-component topology and material orientation design method, aiming to determine continuous fibers for each component and conduct simultaneous topology and angle optimization for the fibers [11]. While this method ensures manufacturability by maintaining continuity for each component, they require predetermined component numbers, leading to reduced design flexibility. Luo et al. [12] proposed a relatively versatile simultaneous optimization method by extending Blasques's approach [13]. However, it does not account for the uniformity required in manufacturing methods like TFP (Tailored Fiber Placement), necessitating post-processing steps. Brampton et al. focused on the manufacturability of Automated Fiber Placement (AFP) and developed a design method solely for angles [14]. Yet, it requires initial angles or preconditioning and is not suitable for simultaneous optimization with topology. Amidst these approaches, Li et al. achieved fiber uniformity by imposing local constraints [15]. However, it incurs high computational cost which results in challenges for practical designs, such as multi-loading problems where the principal stress direction does not align with the fiber orientation.

To address the aforementioned challenges, we propose an integrated two-step approach for topology optimization and fiber arrangement in continuous-fiber composites. The first stage focuses on the concurrent optimization of the structural configuration and anisotropic elastic materials through a level set-based topology optimization and an orientation optimization without considering manufacturability. The structural configuration is represented using a level-set function, which defines a clear boundary surface. On the other hand, a "double angle vector" is introduced as a design variable for the orientation of constructing optimal anisotropic elastic materials. Optimization can be performed in a way that is less likely to suffer from a local optimum solution by utilizing this vector field, a modification of the orientation representation proposed by Nomura et al. [16], rather than directly applying the orientation angle to a design variable. Furthermore, we incorporate the concept of the direction [17,18] for orientation optimization. This direction tensor is defined as the self-diagonal product of unit direction vectors forming an orientation angle with respect to the reference axis, resulting in a more concise formulation of the elastic tensor compared to using the rotation matrix. The partial differential equations based on the reaction–diffusion equation are formulated for simultaneously updating both design variables, i.e., for updating the topology and orientation. While the first phase yields optimal orientations at each node, it does not ensure manufacturability for fabricating continuous fibers. Continuous fibers produced via TFP must be manufactured with continuous and equal spacing between them. In the second phase, we interpret the obtained results from the first stage and reconstruct the manufacturable fiber paths. We note that the design results obtained through the dehomogenization method in the prior works reveal several limitations [19]. Specifically, the mapping employed for deforming the periodic cell in dehomogenization methods is approximately conformal. While this conformity is well-suited for compliance minimization problems characterized by perpendicular bars, it may prove less effective when applied to fiber-reinforced composite designs, where fibers are not necessarily required to align at right angles. In contrast to this, in the fiber reconstruction stage, we introduce a scalar function as a design variable with contour lines representing the optimal fiber paths. We formulate an optimization problem such that the gradient of the scalar function is orthogonal to the given vector or tensor field, and the magnitude of the gradient remains almost constant. These techniques enable us to generate equidistant and continuous fiber paths within the composite structures, thereby maximizing their mechanical performance. The design variable is updated through an adjoint-based optimizer, which is the solution of the reaction–diffusion equation, similar to the first stage. This consistent updating scheme for design variables offers advantages in terms of ease of implementation and parameter studies.

The remainder of this paper is organized as follows. In Section 2, first, we describe the governing equations for the underlying physics. Then we overview the basic concept of the level set-based topology optimization method. Next, the mathematical and physics frames for the parameterization of the orthotropic materials and fiber orientation of anisotropic material are presented. After that, we formulate the two optimization problems. One is for the simultaneous structural configuration and fiber arrangement optimization of stiffness maximization. The other is for the design optimization of generating fiber path lines. Section 3 illustrates the implementation details together with the optimization algorithms. In Section 4, we present several numerical examples to maximize the stiffness under multi-loading conditions, confirming the validity and effectiveness of the proposed methodology. Specifically, concerning the design of fiber path lines, our numerical examples not only demonstrate the efficiency of the proposed method but also showcase its low dependency on initial values through optimization computations initiated from multiple initial conditions. Lastly, the conclusion is provided in Section 5.

2. Formulation

This section shows the mathematical formulations and the optimization methods adopted in this study. First, the governing equations describing the linear elastic problem are presented, and the variables and equations are made dimensionless. Next, we introduce the methodology for simultaneous optimization of topology and orientation for anisotropic elastic materials, which can be applied to the stiffness maximization problem with multi-loading. Finally, we formulate an optimization problem for placing of nearly equally spaced and continuous fibers throughout the structure of the elastic body.

2.1. Governing equations

The deformation of an elastic body is expressed in terms of a state variable defined in the domain Ω to be computed, namely the distribution of displacement $\boldsymbol{u} = \boldsymbol{u}(\boldsymbol{x})$. This study deals with a problem

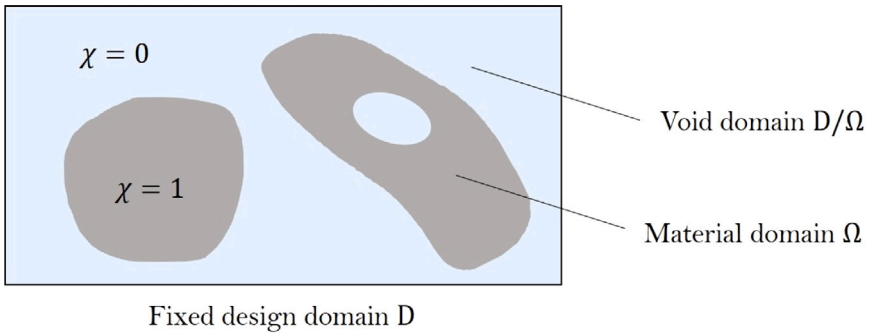

Fig. 1. Concept of topology optimization.

in which the body force, $\bar{\boldsymbol{b}} = \bar{\boldsymbol{b}}(\boldsymbol{x})$, is applied in the domain Ω, the traction, $\bar{\boldsymbol{t}} = \bar{\boldsymbol{t}}(\boldsymbol{x})$, is applied on the boundary Γ_t, and the displacement $\bar{\boldsymbol{u}} = \bar{\boldsymbol{u}}(\boldsymbol{x})$ is fixed on the boundary Γ_u. The state variable satisfies the following governing equations.

$$\nabla \cdot \tilde{\boldsymbol{\sigma}} + \bar{\boldsymbol{b}} = \boldsymbol{0} \quad \text{in } \Omega, \tag{1}$$

$$\boldsymbol{t} = \bar{\boldsymbol{t}} \quad \text{on } \Gamma_t, \tag{2}$$

$$\boldsymbol{u} = \bar{\boldsymbol{u}} \quad \text{on } \Gamma_u; \tag{3}$$

$$\tilde{\boldsymbol{\sigma}} = \tilde{\tilde{\boldsymbol{C}}} : \tilde{\boldsymbol{\epsilon}}. \tag{4}$$

Eq. (1) is the equilibrium equation for elastic bodies where Eq. (4) is the constitutive equation, i.e., Hooke's law. $\tilde{\boldsymbol{\sigma}} = \tilde{\boldsymbol{\sigma}}(\boldsymbol{x})$ is Chauchy's stress tensor, and $\boldsymbol{t} = \tilde{\boldsymbol{\sigma}} \cdot \boldsymbol{n} = \boldsymbol{t}(\boldsymbol{x})$ is the stress vector on the boundary Γ_t, $\boldsymbol{n}$ is the outward unit normal vector on the boundary $\Gamma = \Gamma_t \cup \Gamma_u = \partial\Omega$. $\tilde{\tilde{\boldsymbol{C}}} = \tilde{\tilde{\boldsymbol{C}}}(\boldsymbol{x})$ is the elastic tensor, and $\tilde{\boldsymbol{\epsilon}} = \{(\nabla \boldsymbol{u}) + (\nabla \boldsymbol{u})^{\mathrm{T}}\}/2 = \tilde{\boldsymbol{\epsilon}}(\boldsymbol{x})$ is the strain tensor.

All variables and expressions in this paper are made dimensionless before numerical implementation. Nondimensionalization allows us to determine various parameters required for numerical implementation of the optimization problem, independent of the different cases. Given the representative length, L, the representative displacement, U, and the representative Young's modulus, E_0, the position coordinate, $\boldsymbol{x}$, the displacement, $\boldsymbol{u}$, the strain tensor, $\tilde{\boldsymbol{\epsilon}}$, the stress tensor, $\tilde{\boldsymbol{\sigma}}$, and the stress vector, $\boldsymbol{t}$, are each nondimensionalized as follows,

$$\boldsymbol{x} \leftarrow \frac{\boldsymbol{x}}{L},\ \boldsymbol{u} \leftarrow \frac{\boldsymbol{u}}{U},\ \tilde{\boldsymbol{\epsilon}} \leftarrow \frac{\tilde{\boldsymbol{\epsilon}}}{U/L},\ \tilde{\boldsymbol{\sigma}} \leftarrow \frac{\tilde{\boldsymbol{\sigma}}}{E_0 U/L},\ \boldsymbol{t} \leftarrow \frac{\boldsymbol{t}}{E_0 U/L},\ E \leftarrow \frac{E}{E_0}. \tag{5}$$

The same symbols are then used again for the dimensionless variables and the material properties.

2.2. Level set-based topology optimization method

A fixed design domain D is introduced as shown in Fig. 1 and material distribution in it is represented by using the characteristic function χ as follows:

$$\chi(\boldsymbol{x}) = \begin{cases} 1 & \text{for } \boldsymbol{x} \in \Omega, \\ 0 & \text{for } \boldsymbol{x} \in D \backslash \Omega, \end{cases} \tag{6}$$

where Ω represents the material domain and $D\backslash\Omega$ is the void domain. However, this characteristic function is not guaranteed to be continuous within the fixed design domain, D, which may result in discontinuous structures. One way to solve this problem is to relax or regularize the design space by introducing the level set-based method [20]. The level set function, $\phi(\boldsymbol{x})$, is defined as follows:

$$\begin{cases} 0 < \phi(\boldsymbol{x}) \le 1 & \text{for } \boldsymbol{x} \in \Omega \backslash \partial\Omega, \\ \phi(\boldsymbol{x}) = 0 & \text{for } \boldsymbol{x} \in \partial\Omega, \\ -1 \le \phi(\boldsymbol{x}) < 0 & \text{for } \boldsymbol{x} \in D \backslash \Omega. \end{cases} \tag{7}$$

In this paper, we introduce the smoothed Heaviside function, $H_\delta(\phi)$ defined as follows:

$$H_\delta(\phi) = \begin{cases} 0 & \text{for } -1 \le \phi < -\delta, \\ \frac{1}{2} + \frac{15}{16}\frac{\phi}{\delta} - \frac{5}{8}(\frac{\phi}{\delta})^3 + \frac{3}{16}(\frac{\phi}{\delta})^5 & \text{for } -\delta \le \phi \le \delta, \\ 1 & \text{for } \delta < \phi \le 1. \end{cases} \tag{8}$$

Then, we define the smoothed material distribution or density as $\rho(\phi) = H_\delta(\phi)$. The Young's modulus can be defined with the density, $\rho(\phi)$, as follows:

$$E(\rho(\phi)) = (1 - d)\rho(\phi) + d. \tag{9}$$

Originally, the value of Young's modulus is zero in the void domain $D\backslash\Omega$. In order to avoid the breakdown of the calculation for the solution of the equilibrium equation for elastic bodies, we set the positive constant value, d, which is small enough.

2.3. Orientation optimization

2.3.1. Elasticity tensor of orthotropic materials

This study deals with the deformation problem of elastic bodies with two-dimensional orthotropic material properties. First, suppose that a two-dimensional orthotropic elastic body is aligned along with the coordinate system, meaning that the principal direction of this elastic body corresponds to the first reference axis (x-axis). Let $\tilde{\boldsymbol{C}}^{\text{axis-alin}}$ be the fourth rank elasticity tensor, then its Voigt expression $\tilde{\boldsymbol{C}}^{\text{axis-align}}$ is obtained by taking the inverse of the compliance matrix, $\tilde{\boldsymbol{S}}$, as follows:

$$\tilde{\boldsymbol{C}}^{\text{axis-align}} = \tilde{\boldsymbol{S}}^{-1} = \begin{bmatrix} \frac{E_1}{1-\nu_A\nu_H} & \frac{\nu_H E_A}{1-\nu_A\nu_H} & 0 \\ & \frac{E_2}{1-\nu_A\nu_H} & 0 \\ (\text{sym.}) & & G \end{bmatrix} := \begin{bmatrix} C_{1111} & C_{1122} & 0 \\ & C_{2222} & 0 \\ (\text{sym.}) & & C_{1212} \end{bmatrix}, \tag{10}$$

$$\tilde{\boldsymbol{S}} = \begin{bmatrix} \frac{1}{E_1} & -\frac{\nu_A}{E_A} & 0 \\ & \frac{1}{E_2} & 0 \\ (\text{sym.}) & & \frac{1}{G} \end{bmatrix}, \tag{11}$$

where E_1 and E_2 are Young's moduli of the elastic body in the principal (along the reference axis) and secondary (orthogonal to the reference axis) directions, respectively, and E_A is their arithmetic mean $(E_1 + E_2)/2$. ν_A and ν_H are the arithmetic mean $(\nu_{12} + \nu_{21})/2$ and harmonic mean $\{(\nu_{12}^{-1} + \nu_{21}^{-1})/2\}^{-1}$ of two Poisson ratios ν_{12} and ν_{21}, respectively. G is the rigidity modulus. Generally, in a two-dimensional orthotropic elastic body, the four independent properties are two Young's moduli E_1, E_2, Poisson's ratio ν_{12} (or ν_{21},) and the rigidity modulus G. But in

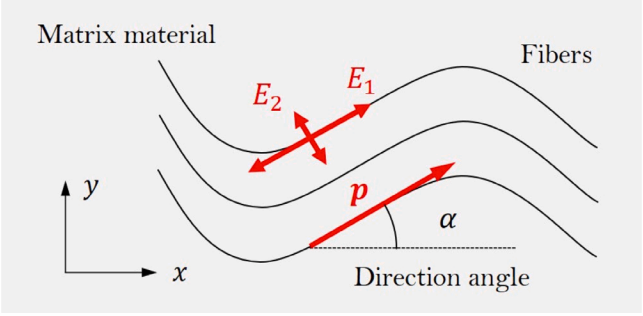

Fig. 2. Model of fiber-reinforced composite material.

this research, G is supposed to be dependent on the other properties, given by the following expression.

$$G = G_H = \left(\frac{G_1^{-1} + G_2^{-1}}{2} \right)^{-1} = \frac{E_1 E_2}{E_1 + E_2 + \nu_{21} E_1 + \nu_{12} E_2}. \tag{12}$$

where G_1 and G_2 are rigidity moduli of two hypothetical isotropic elastic bodies, expressed as $G_1 = E_1/2(1+\nu_{12})$, and $G_2 = E_2/2(1+\nu_{21})$, respectively.

2.3.2. Orientation representation of anisotropic material with direction tensor

Here is the definition of the fourth rank elasticity tensor $\tilde{\tilde{C}}_0$ for two-dimensional arbitrarily oriented orthotropic material. The elasticity tensor $\tilde{\tilde{C}}_0$ is expressed by using the components of the elastic tensor, $\tilde{C}^{\text{axis-align}}$ in Eq. (10) and the second rank direction tensor $\tilde{\boldsymbol{W}}$ defined later, as follows:

$$\begin{aligned} \tilde{\tilde{C}}_0 \left(\tilde{\boldsymbol{W}} \right) = & \left(C_{1111} + C_{2222} - 2C_{1122} - 4C_{1212} \right) \left(\tilde{\boldsymbol{W}} \otimes \tilde{\boldsymbol{W}} \right) + C_{1212} \left(\tilde{\tilde{\boldsymbol{J}}} + \tilde{\tilde{\boldsymbol{J}}}^{\mathrm{T}} \right) \\ & + \left(C_{2222} - 2C_{1212} \right) \left(\tilde{\boldsymbol{I}} \otimes \tilde{\boldsymbol{I}} \right) + \left(-C_{2222} + C_{1122} + 2C_{1212} \right) \\ & \times \left(\tilde{\boldsymbol{I}} \otimes \tilde{\boldsymbol{W}} + \tilde{\boldsymbol{W}} \otimes \tilde{\boldsymbol{I}} \right), \end{aligned} \tag{13}$$

where $\tilde{\boldsymbol{I}}$ and $\tilde{\tilde{\boldsymbol{J}}}$ are the second rank identity tensor $\tilde{\boldsymbol{I}} := \left[\delta_{ij}\right]$ and the fourth rank identity tensor $\tilde{\tilde{\boldsymbol{J}}} := \left[\delta_{ik}\delta_{jl}\right]$, respectively. Also, $\tilde{\tilde{\boldsymbol{J}}}^{\mathrm{T}}$ is one of the transposes of $\tilde{\tilde{\boldsymbol{J}}}$ and is defined as $\boldsymbol{J}^{\mathrm{T}}_{ijkl} = \boldsymbol{J}_{jikl}$.

Next, let us consider the second-order direction tensor $\tilde{\boldsymbol{W}}$, which is the only variable contained in Eq. (13). When the fiber direction angle of a two-dimensional orthotropic material is represented by $\alpha = \alpha(\boldsymbol{x})$ as shown in Fig. 2, one of the unit vectors in the direction along the fiber is expressed as $\boldsymbol{p} = [\cos\alpha, \sin\alpha]^{\mathrm{T}} = \boldsymbol{p}(\boldsymbol{x})$, which is named "direction vector" in this paper. The second rank direction tensor $\tilde{\boldsymbol{W}} = \tilde{\boldsymbol{W}}(\boldsymbol{x})$ is defined as the self-dyadic product of the unit vector $\boldsymbol{p}$ as follows:

$$\tilde{\boldsymbol{W}} = \boldsymbol{p} \otimes \boldsymbol{p} = \begin{bmatrix} \cos^2\alpha & \sin\alpha\cos\alpha \\ \sin\alpha\cos\alpha & \sin^2\alpha \end{bmatrix}, \tag{14}$$

which is named "direction tensor" in this paper.

Here, we discuss the design variables for expressing this direction tensor. A method such as the CFAO [7–9] (Continuous Fiber Angle Optimization), in which the fiber direction angle, α, is directly assigned as a design variable, can be a candidate. However, as claimed by Stegmann et al. [10,21], the CFAO method has the disadvantage of being prone to local optima. Furthermore, when handling direction angles, there is the difficulty of performing proper regularization. The elasticity tensor $\tilde{\tilde{C}}_0$ for direction angle $\alpha = \alpha_0$ identifies with the cases of $\alpha = \alpha_0 \pm n\pi$, due to the periodicity of angle. Hence, we adopted the idea of the orientation representation for anisotropic materials proposed by Nomura et al. [16]. The design variable is defined as the unit vector $\boldsymbol{\vartheta} = [\cos\theta, \sin\theta]^{\mathrm{T}} = [\varsigma, \zeta]^{\mathrm{T}} = \boldsymbol{\vartheta}(\boldsymbol{x})$, where θ is set as the following equation so that this design variable $\boldsymbol{\vartheta}$ can be regarded to have the period 2π,

$$\theta = 2\alpha. \tag{15}$$

The angle θ can be interpreted as the direction angle of the design variables $\boldsymbol{\vartheta}$ toward the reference axis, so this design variable $\boldsymbol{\vartheta}$ is named the "double angle direction vector" in this paper. From Eqs. (14) and (15), the direction tensor $\tilde{\boldsymbol{W}}(\boldsymbol{\vartheta})$ can be expressed using θ as follows:

$$\tilde{\boldsymbol{W}}(\boldsymbol{\vartheta}) = \frac{1}{2} \begin{bmatrix} 1 + \cos\theta & \sin\theta \\ \sin\theta & 1 - \cos\theta \end{bmatrix}. \tag{16}$$

Note that the double direction angle θ is still periodic and difficult to regularize in the optimization problem as the direction angle α. One of the more appropriate design variables would be each component of the double angle direction vector $\boldsymbol{\vartheta} = [\varsigma, \zeta]^{\mathrm{T}}$. Replacing $\cos\theta$ and $\sin\theta$ in Eq. (16) with ς and ζ, respectively, the elasticity tensor $\tilde{\tilde{\boldsymbol{C}}}_0 = \tilde{\tilde{\boldsymbol{C}}}_0(\tilde{\boldsymbol{W}}(\boldsymbol{\vartheta}))$ can be expressed as:

$$\tilde{\boldsymbol{W}}(\boldsymbol{\vartheta}) = \frac{1}{2} \begin{bmatrix} 1 + \varsigma & \zeta \\ \zeta & 1 - \varsigma \end{bmatrix}. \tag{17}$$

Considering these orientation expressions and the shape representation described in Section 2.2, and further combining Eqs. (9) and (13), we obtain an expression that incorporates the design variable, $\phi, \boldsymbol{\vartheta}$ into the elasticity tensor $\tilde{\tilde{\boldsymbol{C}}} = \tilde{\tilde{\boldsymbol{C}}}(\phi, \boldsymbol{\vartheta})$,

$$\tilde{\tilde{\boldsymbol{C}}}(\phi, \boldsymbol{\vartheta}) = E(\rho(\phi)) \tilde{\tilde{\boldsymbol{C}}}_0(\tilde{\boldsymbol{W}}(\boldsymbol{\vartheta})). \tag{18}$$

In this work, we relax some of the conditions that the double angle direction vector $\boldsymbol{\vartheta}$ originally should satisfy, and allow its norm to be $\|\boldsymbol{\vartheta}\| \leq 1$ only during the process of optimization, as shown in Fig. 3. This allows optimization to be performed flexibly by updating the double angle direction vector $\boldsymbol{\vartheta}$ in directions not only tangential to the unit circle. We discuss the detail in the next section.

2.3.3. Relaxation of the conditions for the orientation design variables

Regarding the orientation representation of anisotropic materials proposed in Section 2.3.2, direction vector $\boldsymbol{p}$, double-angle direction vector $\boldsymbol{\vartheta}$, and direction tensor $\tilde{\boldsymbol{W}}$ should satisfy the following fundamental conditions:

$$\|\boldsymbol{p}\| = \sqrt{\cos^2\alpha + \sin^2\alpha} = 1, \tag{19}$$

$$\|\boldsymbol{\vartheta}\| = \sqrt{\varsigma^2 + \zeta^2} = \sqrt{\cos^2\theta + \sin^2\theta} = 1, \tag{20}$$

$$\mathrm{tr}\tilde{\boldsymbol{W}} = \|p\|^2 = \|\boldsymbol{\vartheta}\|^2 = 1, \tag{21}$$

$$\det\tilde{\boldsymbol{W}} = \cos^2\alpha\sin^2\alpha - (\cos\alpha\sin\alpha)^2 = 0. \tag{22}$$

Eqs. (19) to (21) ensure that the norm of direction vector $\boldsymbol{p}$ (or double-angle direction vector $\boldsymbol{\vartheta}$) is 1. These conditions should be satisfied in the final stage of optimization, but not necessarily satisfied during the intermediate process of optimization. As shown in Fig. 3, the norm should rather be allowed to be less than 1 for numerical advantages. In short, during the optimization procedure, we should permit $\mathrm{tr}\tilde{\boldsymbol{W}} < 1$, although it corresponds to a reduction in the stiffness of the elastic body. On the other hand, Eq. (22) ensures that the direction tensor $\tilde{\boldsymbol{W}}$ is defined as a self-dyadic product of direction vector $\boldsymbol{p}$, as in Eq. (14). This condition should be always satisfied in the optimization procedures. Considering these factors, the direction tensor is modified as follows so that Eq. (22) is always valid during the optimization process, and furthermore, the Eqs. (19) to (21) are also valid at the end of the optimization.

$$\tilde{\boldsymbol{W}} = \frac{\min(\|\boldsymbol{\vartheta}\|, 1)}{2\|\boldsymbol{\vartheta}\|} \begin{bmatrix} \|\boldsymbol{\vartheta}\| + \varsigma & \zeta \\ \zeta & \|\boldsymbol{\vartheta}\| - \zeta \end{bmatrix}, \tag{23}$$

$$\mathrm{tr}\tilde{\boldsymbol{W}} = \min(\|\boldsymbol{\vartheta}\|, 1) \leq 1, \tag{24}$$

$$\det\tilde{\boldsymbol{W}} = 0. \tag{25}$$

Note that when dealing with the stiffness maximization problem, it is expected that $\mathrm{tr}\tilde{\boldsymbol{W}}$ will naturally converge to 1 in the final stage of the optimization. Since the "min" function is used for $\tilde{\boldsymbol{W}}$ in Eq. (23), there is a problem of non-differentiability at $\|\boldsymbol{\vartheta}\| = 1$.

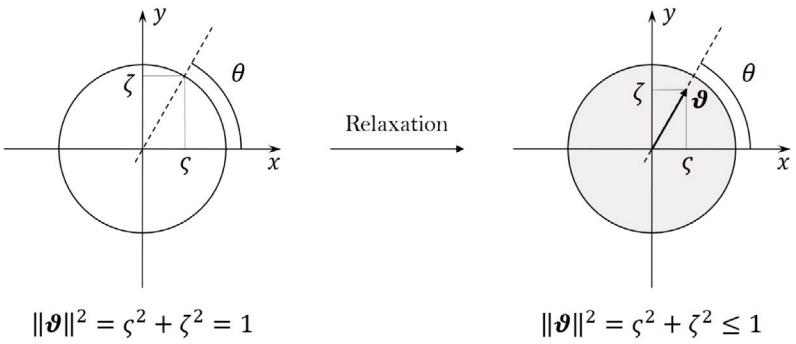

Fig. 3. Cartesian representation and its relaxation.

Then, as in the discussion in Eq. (8), we replace $\min(\|\boldsymbol{\vartheta}\|, 1)$ with $H_\delta(\|\boldsymbol{\vartheta}\| - 1/2, 1/2)$ as follows:

$$\tilde{\boldsymbol{W}} = \frac{1}{2\|\boldsymbol{\vartheta}\|} H_\delta(\|\boldsymbol{\vartheta}\| - \frac{1}{2}, \frac{1}{2}) \begin{bmatrix} \|\boldsymbol{\vartheta}\| + \varsigma & \zeta \\ \zeta & \|\boldsymbol{\vartheta}\| - \varsigma \end{bmatrix}, \tag{26}$$

$$= \frac{1}{\|\boldsymbol{\vartheta}\|} \{\frac{1}{4} + \frac{15}{16}(\|\boldsymbol{\vartheta}\| - \frac{1}{2}) - \frac{5}{2}(\|\boldsymbol{\vartheta}\| - \frac{1}{2})^3 + 3(\|\boldsymbol{\vartheta}\| - \frac{1}{2})^5\} \begin{bmatrix} \|\boldsymbol{\vartheta}\| + \varsigma & \zeta \\ \zeta & \|\boldsymbol{\vartheta}\| - \varsigma \end{bmatrix}, \tag{27}$$

Finally, we penalize the norm of the double-angle direction vector $\boldsymbol{\vartheta}$ to be upper bounded with 1, as explained in Section 2.4.2.

2.4. Design problem of stiffness maximization

2.4.1. Mathematical optimization model

Let us consider the stiffness maximization problem, which is one of the most general optimal design problems for elastic materials. The optimization problem considered in this paper is formulated as a multi-loading problem. In other words, we assume that a single elastic body is subjected to different n ways of loads, and consider an optimization problem that attempts to obtain a set of design variables, ϕ and $\boldsymbol{\vartheta}$ that yields great performance for all of them. Subject to the governing equations, Eqs. (1) to (4) and the upper bounded volume constraint of the material, the mean compliance minimization problem of the elastic body is formulated as follows:

$$\underset{\phi,\boldsymbol{\vartheta}}{\text{minimize}}\ \bar{F}[\phi, \boldsymbol{\vartheta}] = \max\left(F_1, F_2, \dots, F_n\right) + f_\phi + f_{\boldsymbol{\vartheta}}, \tag{28}$$

$$F_i[\phi, \boldsymbol{\vartheta}] = \int_D \bar{\boldsymbol{b}}_i \cdot \boldsymbol{u}_i \mathrm{d}D + \int_{\Gamma_{t_i}} \bar{\boldsymbol{t}}_i \cdot \boldsymbol{u} \mathrm{d}\Gamma - \int_{\Gamma_{u_i}} \boldsymbol{t}_i \cdot \bar{\boldsymbol{u}}_i \mathrm{d}\Gamma, \tag{29}$$

$$f_\phi[\phi] = \frac{\tau_\phi}{2} \int_D \|\nabla\phi\|^2 \mathrm{d}D, \tag{30}$$

$$f_{\boldsymbol{\vartheta}}[\boldsymbol{\vartheta}] = \frac{\tau_{\boldsymbol{\vartheta}}}{4} \int_D \{\nabla\boldsymbol{\vartheta} + (\nabla\boldsymbol{\vartheta})^{\mathrm{T}}\} : \{\nabla\boldsymbol{\vartheta} + (\nabla\boldsymbol{\vartheta})^{\mathrm{T}}\} \mathrm{d}D, \tag{31}$$

$$\text{subject to}\quad G[\phi] = \int_D \rho \mathrm{d}D - \bar{V} \leq 0, \tag{32}$$

$$\int_D \tilde{\boldsymbol{\sigma}}_i : \hat{\tilde{\boldsymbol{\varepsilon}}}_i \mathrm{d}D + \int_D \bar{\boldsymbol{b}}_i \cdot \hat{\boldsymbol{u}}_i \mathrm{d}D = \int_{\Gamma_t} \bar{\boldsymbol{t}}_i \cdot \hat{\boldsymbol{u}}_i \mathrm{d}\Gamma. \tag{33}$$

We deal with the multi-loading problem of minimizing the maximum of the n principal objective functionals F_i defined in Eq. (29). In the right hand side of Eq. (29), the first term represents the minimization of the work done by the body force $\bar{\boldsymbol{b}}_i$ on the elastic body in the domain D, the second term represents the minimization of the displacement $\boldsymbol{u}_i$ at the boundary with fixed stress, Γ_{t_i}, and the third term represents the maximization of the stress $\boldsymbol{t}_i$ at the boundary with fixed displacement, Γ_{u_i}. f_ϕ and $f_{\boldsymbol{\vartheta}}$ are auxiliary objective functionals for regularizing the design variables ϕ and $\boldsymbol{\vartheta}$, respectively. Eq. (32) represents the upper bounded volume constraint of the material, and $\bar{V}$ is its upper bound. Eq. (33) is the weak form of the governing equation for an elastic body subjected to multiple loads, where $\hat{\boldsymbol{u}}_i$ is the vector of a test function and $\hat{\tilde{\boldsymbol{\varepsilon}}}_i$ is defined as $\hat{\tilde{\boldsymbol{\varepsilon}}}_i = \{(\nabla\hat{\boldsymbol{u}}_i) + (\nabla\hat{\boldsymbol{u}}_i)^{\mathrm{T}}\}/2$.

2.4.2. Updating scheme for design variables

We describe in detail how to update the design variables ϕ and $\boldsymbol{\vartheta}$ for the optimization problem of stiffness maximization. First, the constrained optimization problem outlined in Section 2.4.1 is replaced with an unconstrained optimization problem by the Lagrange multiplier method.

Letting $F_j = F_j[\phi(\boldsymbol{x}), \boldsymbol{\vartheta}(\boldsymbol{x})]$ be the maximum of n principal objective functionals F_i's shown in Eq. (29), and defining Lagrangian $\mathcal{F} = \mathcal{F}[\phi(\boldsymbol{x}), \boldsymbol{\vartheta}(\boldsymbol{x}); \lambda_G]$ using F_j, the upper volume constraint functional G in Eq. (32), and its Lagrange multiplier λ_G, the unconstrained optimization problem is expressed as follows:

$$\underset{\phi,\boldsymbol{\vartheta}}{\text{minimize}}\ \mathcal{F}[\phi(\boldsymbol{x}), \boldsymbol{\vartheta}(\boldsymbol{x}); \lambda_G] = F_j[\phi(\boldsymbol{x}), \boldsymbol{\vartheta}(\boldsymbol{x})] + \lambda_G G[\phi(\boldsymbol{x})]. \tag{34}$$

At this time, the Karush-Kuhn–Tucker (KKT) condition is expressed as follows:

$$\begin{cases} S_\phi(\boldsymbol{x}; \lambda_G) = \dfrac{\delta\mathcal{F}[\phi(\boldsymbol{x}), \boldsymbol{\vartheta}(\boldsymbol{x}); \lambda_G]}{\delta\phi(\boldsymbol{x})} = S_{\phi_{F_j}}(\boldsymbol{x}) + \lambda_G S_{\phi_G}(\boldsymbol{x}) = 0, \\ \boldsymbol{S}_{\boldsymbol{\vartheta}}(\boldsymbol{x}; \lambda_G) = \dfrac{\delta\mathcal{F}[\phi(\boldsymbol{x}), \boldsymbol{\vartheta}(\boldsymbol{x}); \lambda_G]}{\delta\boldsymbol{\vartheta}(\boldsymbol{x})} = \boldsymbol{S}_{\boldsymbol{\vartheta}_{F_j}}(\boldsymbol{x}) + \lambda_G \boldsymbol{S}_{\boldsymbol{\vartheta}_G}(\boldsymbol{x}) = \boldsymbol{0}, \\ \lambda_G G[\phi(\boldsymbol{x})] = 0,\ \lambda_G \geq 0,\ G[\phi(\boldsymbol{x})] \leq 0. \end{cases} \tag{35}$$

Originally, $S_{\phi_{F_j}}(\boldsymbol{x})$, $\boldsymbol{S}_{\boldsymbol{\vartheta}_{F_j}}(\boldsymbol{x})$ and $S_{\phi_G}(\boldsymbol{x})$, $\boldsymbol{S}_{\boldsymbol{\vartheta}_G}(\boldsymbol{x})$ are the functional derivatives of objective functional $F_j[\phi(\boldsymbol{x}), \boldsymbol{\vartheta}(\boldsymbol{x})]$ and constraint functional $G[\phi(\boldsymbol{x})]$, respectively, by the design variable $\phi(\boldsymbol{x})$, $\boldsymbol{\vartheta}(\boldsymbol{x})$. In this research, they are partially replaced with alternative expressions. Here, $S_{\phi_{F_j}}$, $\boldsymbol{S}_{\boldsymbol{\vartheta}_{F_j}}$, S_{ϕ_G}, $\boldsymbol{S}_{\boldsymbol{\vartheta}_G}$ can be represented as follows:

$$S_{\phi_{F_j}}(\boldsymbol{x}) = -\tilde{\boldsymbol{\varepsilon}}_j(\boldsymbol{x}) : \tilde{\tilde{\boldsymbol{C}}}(\boldsymbol{x}) : \tilde{\boldsymbol{\varepsilon}}_j(\boldsymbol{x}), \tag{36}$$

$$\boldsymbol{S}_{\boldsymbol{\vartheta}_{F_j}}(\boldsymbol{x}) = -\tilde{\boldsymbol{\varepsilon}}_j(\boldsymbol{x}) : \frac{\partial\tilde{\tilde{\boldsymbol{C}}}(\boldsymbol{x})}{\partial\boldsymbol{\vartheta}(\boldsymbol{x})} : \tilde{\boldsymbol{\varepsilon}}_j(\boldsymbol{x}), \tag{37}$$

$$S_{\phi_G}(\boldsymbol{x}) = \frac{\delta G[\phi(\boldsymbol{x})]}{\delta\rho(\boldsymbol{x})} = 1, \tag{38}$$

$$\boldsymbol{S}_{\boldsymbol{\vartheta}_G}(\boldsymbol{x}) = \frac{\delta G[\phi(\boldsymbol{x})]}{\delta\boldsymbol{\vartheta}(\boldsymbol{x})} = \boldsymbol{0}. \tag{39}$$

$S_{\phi_{F_j}}$ in Eq. (36) is the design sensitivity for the level-set based topology optimization following the lead of Yamada et al. [20]. $\boldsymbol{S}_{\boldsymbol{\vartheta}_{F_j}}$ in Eq. (37) is the design sensitivity for the orientation optimization, which is also derived via the adjoint variable method as Eq. (36). S_{ϕ_G} and $\boldsymbol{S}_{\boldsymbol{\vartheta}_G}$ in Eqs. (38) and (39), respectively, are the functional derivatives with respect to ρ and $\boldsymbol{\vartheta}$ of the volume upper bound constraint functional G in Eq. (32).

The candidate for the optimal solution of the mean compliance minimization problem is the design variable ϕ, $\boldsymbol{\vartheta}$ that satisfies the KKT condition, but it is difficult to find this optimal solution directly from the condition in Eq. (35). Hence, we employ the time evolution equation to obtain the optimal solution. In other words, a fictitious time t is introduced, proper initial values are given, and the level-set function is temporally updated according to the following reaction–diffusion equation to obtain candidate design variables ϕ, $\boldsymbol{\vartheta}$ that can

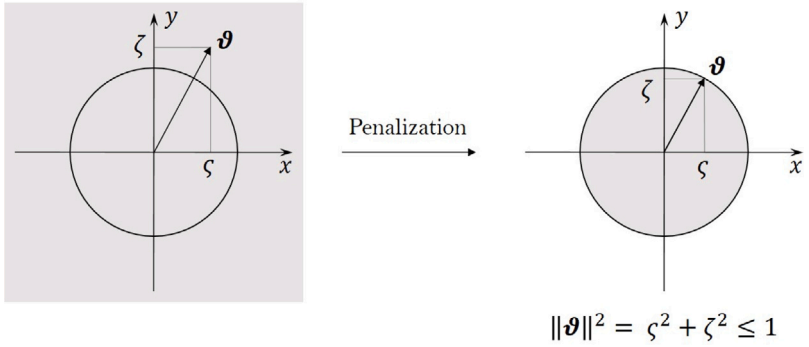

Fig. 4. Penalization for the norm of double-angle direction vector.

be the optimal solution. In solving the time evolution equation, appropriate Neumann or Dirichlet boundary conditions are imposed on $\Gamma = \partial D$. Moreover, adding the auxiliary terms described later, the time evolution equation can be expressed as a reaction–diffusion equation as follows:

$$\begin{cases} m_\phi \dfrac{\partial \phi(\boldsymbol{x},t)}{\partial t} = -S_\phi(\boldsymbol{x},t) + \tau_\phi \nabla^2 \phi(\boldsymbol{x},t) + P_\phi[\phi(\boldsymbol{x},t)] & \text{in } D, \\ \dfrac{\partial \phi(\boldsymbol{x},t)}{\partial n} = 0 & \text{on } \Gamma, \\ m_{\boldsymbol{\vartheta}} \dfrac{\partial \boldsymbol{\vartheta}(\boldsymbol{x},t)}{\partial t} = -\boldsymbol{S}_{\boldsymbol{\vartheta}}(\boldsymbol{x},t) + \tau_{\boldsymbol{\vartheta}} \boldsymbol{\nabla} \cdot (\boldsymbol{\nabla}\boldsymbol{\vartheta}(\boldsymbol{x},t) + \{\boldsymbol{\nabla}\boldsymbol{\vartheta}(\boldsymbol{x},t)\}^{\mathrm{T}}) + \boldsymbol{P}_{\boldsymbol{\vartheta}}[\boldsymbol{\vartheta}(\boldsymbol{x},t)] & \text{in } D, \\ \dfrac{\partial \boldsymbol{\vartheta}(\boldsymbol{x},t)}{\partial n} = \boldsymbol{0} & \text{on } \Gamma, \end{cases} \tag{40}$$

where $m_\phi, m_{\boldsymbol{\vartheta}}$ on the left-hand side of the first and third equations are constants. The second term on the right hand side of the first equation is the sensitivity of the auxiliary objective functional f_ϕ for ϕ in Eq. (30), and the second term on the right side of the third equation is the sensitivity of the auxiliary objective functional f_θ for $\boldsymbol{\vartheta}$ in Eq. (31). τ_ϕ and $\tau_{\boldsymbol{\vartheta}}$ are the regular coefficients for each design variables. They are well-known parameters that can be used to control the complexity of the optimal structures [22]. The third terms P_ϕ and $\boldsymbol{P}_{\boldsymbol{\vartheta}}$ on the right side of the first and third equations are the penalty terms. These terms are introduced so that the design variable ϕ and $\boldsymbol{\vartheta}$ are updated within the upper bound of the norm of ϕ and $\boldsymbol{\vartheta}$ as far as possible, and expressed as follows:

$$P_\phi[\phi(\boldsymbol{x},t)] = \Lambda_\phi\{\phi_{\mathrm{lub}}(\boldsymbol{x},t) - \phi(\boldsymbol{x},t)\}; \quad \phi_{\mathrm{lub}}(\boldsymbol{x},t) = \frac{\phi(\boldsymbol{x},t)}{\max(1,|\phi|)}, \tag{41}$$

$$\boldsymbol{P}_{\boldsymbol{\vartheta}}[\boldsymbol{\vartheta}(\boldsymbol{x},t)] = \Lambda_{\boldsymbol{\vartheta}}\{\boldsymbol{\vartheta}_{\mathrm{mub}}(\boldsymbol{x},t) - \boldsymbol{\vartheta}(\boldsymbol{x},t)\}; \quad \boldsymbol{\vartheta}_{\mathrm{mub}}(\boldsymbol{x},t) = \frac{\boldsymbol{\vartheta}(\boldsymbol{x},t)}{\max(1,\|\boldsymbol{\vartheta}\|)}. \tag{42}$$

The coefficients Λ_ϕ, $\Lambda_{\boldsymbol{\vartheta}}(\gg 1)$ on the right hand side of Eqs. (41) and (42) are parameters that adjust the contribution of the penalty term to the overall reaction–diffusion equation, Eq. (40). The larger the contribution of the penalty term P_ϕ, the more exactly the level set function ϕ satisfies $-1 \leq \phi \leq 1$, which makes diffusion by f_ϕ in Eq. (30) work only at the interface between the material and void domain. Similarly, the larger the contribution of the penalty term $\boldsymbol{P}_{\boldsymbol{\vartheta}}$, the closer its norm approaches to 1 while maintaining the orientation of double-angle direction vector $\boldsymbol{\vartheta}$, as shown in Fig. 4.

2.5. Design problem of generating fiber path lines

2.5.1. Mathematical optimization model

We show how to display the actual fiber arrangement by path lines which are generated from the distribution of the double-angle direction vector $\boldsymbol{\vartheta}$ obtained by the structural optimization method described in Section 2.4.1. This method is effective in the design phase of mechanical products made of fiber-reinforced composites such as CFRP. Generated fiber arrangement is both highly rigid and easy to manufacture, because the fibers can be controlled to be equally spaced and continuous and not to intersect each other.

The path line of fibers is obtained by attributing it to an optimization problem. A scalar function $\psi = \psi(\boldsymbol{x})$ is defined as a design variable of the optimization problem in the fixed design domain, D. Then, let this scalar function ψ be optimized so that its contours follow the given vector field (or tensor field). Given the direction tensor $\tilde{\boldsymbol{W}} = \boldsymbol{p} \otimes \boldsymbol{p}$, this can be done by optimizing the scalar function ψ so that $\boldsymbol{\nabla}\psi \cdot \boldsymbol{p} \to 0$ (or $(\boldsymbol{\nabla}\psi \cdot \boldsymbol{p})^2 = \{(\boldsymbol{\nabla}\psi)(\boldsymbol{\nabla}\psi)^{\mathrm{T}}\} : \tilde{\boldsymbol{W}} \to 0$).

The above optimization problem is formulated as follows:

$$\underset{\psi}{\text{minimize}}\, \bar{F}_\psi[\psi] = F_{\mathrm{orth}} + F_{\mathrm{df}} + f_\psi, \tag{43}$$

$$F_{\mathrm{orth}}[\psi] = \frac{C_{\mathrm{orth}}}{2} \int_D \rho \left(\{(\boldsymbol{\nabla}\psi)(\boldsymbol{\nabla}\psi)^{\mathrm{T}}\} : \tilde{\boldsymbol{W}} \right) \mathrm{d}D, \tag{44}$$

$$F_{\mathrm{df}}[\psi] = \frac{C_{\mathrm{df}}}{4} \int_D \rho (1 - \|\nabla\psi\|^2)^2 \mathrm{d}D, \tag{45}$$

$$f_\psi[\psi] = \frac{\tau_\psi}{2} \int_D \|\boldsymbol{\nabla}\psi\|^2 \mathrm{d}D, \tag{46}$$

where F_{orth} is the objective functional that requires the gradient vector of the scalar function ψ to be orthogonal to direction tensor $\tilde{\boldsymbol{W}}$. F_{df} is the objective functional that requires the scalar function ψ contours to be equally spaced. Note that in these two objective functionals, the integrand on the right-hand side is multiplied by the density function ρ, since the objective in this study is to design the fiber arrangement in the material domain Ω by scalar function ψ. f_ψ is an auxiliary objective functional that intends to regularize the design variable ψ. When the optimization is performed with the objective functionals in Eqs. (43) to (46), however, only the gradient $\boldsymbol{\nabla}\psi$ of the scalar function ψ can be determined. In other words, if certain $\psi = \psi'(\boldsymbol{x})$ is a candidate solution of the above optimization problem, then $\psi = \psi'(\boldsymbol{x}) + \psi_0$ should also be a candidate. To avoid this problem, we assign the point constraint $\psi(\boldsymbol{x}_0) = \psi_0$ at $\boldsymbol{x} = \boldsymbol{x}_0$ in the domain.

2.5.2. Updating scheme for design variables

We describe in detail how to update the design variable ψ for the optimization problem of generating fiber path lines. Similarly for the optimization problem of producing fiber path lines, it is difficult to directly obtain the best design variable ψ from Eqs. (43) to (46). The optimization problem is replaced with that of solving the time evolution equation to update the design variable and find the optimal solution:

$$\begin{cases} m_\psi \dfrac{\partial \psi(\boldsymbol{x},t)}{\partial t} = -S_{F_{\mathrm{orth}}}(\boldsymbol{x},t) - S_{F_{\mathrm{df}}}(\boldsymbol{x},t) - S_{f_\psi}(\boldsymbol{x},t) & \text{in } D, \\ \dfrac{\partial \psi(\boldsymbol{x},t)}{\partial n} = 0 & \text{on } \Gamma, \\ \psi(\boldsymbol{x},t) = \psi_0 & \text{at } \boldsymbol{x} = \boldsymbol{x}_0. \end{cases} \tag{47}$$

Also in this time evolution equation, the Neumann boundary condition is imposed like in Eq. (40). The third equation provides a point constraint for the design variable $\psi(\boldsymbol{x},t)$ to have fixed value ψ_0 at $\boldsymbol{x} = \boldsymbol{x}_0$, thereby preventing the optimization problem from being ill-posed. In

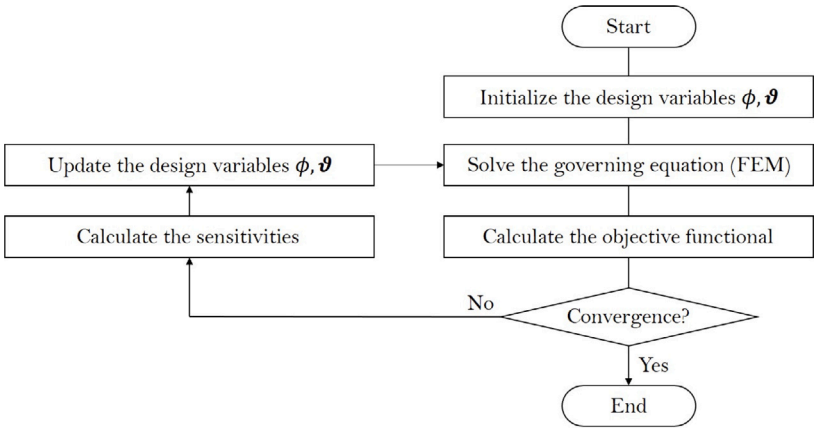

Fig. 5. Flowchart of the mean compliance minimization problem.

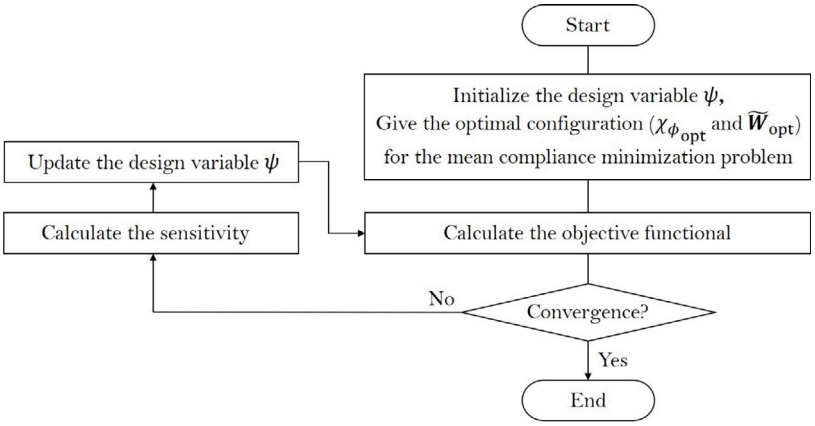

Fig. 6. Flowchart of the generation problem for the fiber path lines.

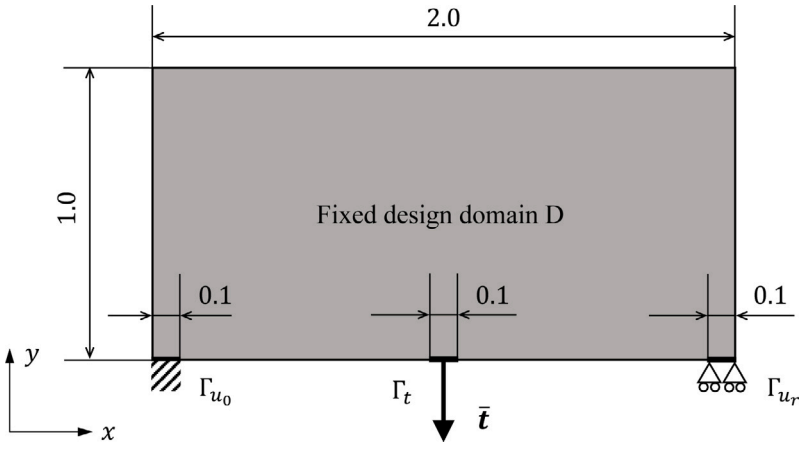

Fig. 7. Design settings for the bridge problem.

addition, $S_{F_{\text{orth}}}$, $S_{F_{\text{df}}}$ and S_{f_ψ} in the right side of the first equation are the sensitivity to the scalar function ψ for the objective functionals F_{orth}, F_{df} and f_{diff} shown in Eqs. (44) to (46), respectively, and can be expressed as follows:

$$S_{F_{\text{orth}}}(\boldsymbol{x}) = \frac{\delta F_{\text{orth}}[\psi(\boldsymbol{x})]}{\delta \psi(\boldsymbol{x})} = -C_{\text{orth}}\rho(\boldsymbol{x})\boldsymbol{\nabla}\cdot(\tilde{\boldsymbol{W}}(\boldsymbol{x})\cdot\{\boldsymbol{\nabla}\psi(\boldsymbol{x})\}), \tag{48}$$

$$S_{F_{\text{df}}}(\boldsymbol{x}) = C_{\text{df}}\rho(\boldsymbol{x})\nabla\cdot\{(1-|\nabla\psi|^2)\nabla\psi\}, \tag{49}$$

$$S_{f_\psi}(\boldsymbol{x}) = \frac{\delta f_\psi[\psi(\boldsymbol{x})]}{\delta \psi(\boldsymbol{x})} = -\tau_\psi \boldsymbol{\nabla}^2\psi(\boldsymbol{x}). \tag{50}$$

3. Implementation details

3.1. Optimization algorithm for stiffness maximization problem

For the stiffness maximization problem shown in Section 2.4.1, the flowchart of the algorithm in the proposed method is shown in Fig. 5. First, we set the level set function $\phi = \phi_{\text{init}}(\boldsymbol{x})$ representing the initial structure and the double-angle direction vector $\vartheta = \vartheta_{\text{init}}(\boldsymbol{x}) = |\varsigma_{\text{init}}(\boldsymbol{x}), \zeta_{\text{init}}(\boldsymbol{x})|^{\text{T}}$ representing the initial direction. Next, the governing equations are solved by the finite element method and the objective

Fig. 8. Optimal configuration for the bridge problem.

functional is evaluated. If the objective value is converged, the optimization procedure is terminated. If not, the sensitivity to the level-set function ϕ and the double-angle direction vector $\boldsymbol{\vartheta}$ are calculated and the design variables are updated simultaneously. It should be noted here that although it is possible to update the two design variables one by one, it has been reported that simultaneously updating the design variables enables the convergence of the objective functionals to smaller values and the derivation of superior optimized results [17]. The detail is discussed in a later section. Then, it returns to the steps of solving the governing equations and evaluating the objective functional. Iterating the above procedure, we obtain the level-set function $\phi = \phi_{\text{opt}}(\boldsymbol{x})$, which represents a candidate for the optimal structure, and the double-angle direction vector $\boldsymbol{\vartheta} = \boldsymbol{\vartheta}_{\text{opt}}(\boldsymbol{x})$, which represents a candidate for the optimal orientation. In this research, a series of these optimization procedures were implemented in COMSOL Multiphysics 5.6 and the computations were performed.

3.2. Optimization algorithm for generating fiber path lines

For the problem of generating fiber path lines shown in Section 2.5.1, the flowchart of the algorithm in the proposed method is shown in Fig. 6. First, the initial distribution of the scalar function $\psi = \psi_{\text{init}}(\boldsymbol{x})$ is set, and then the optimized design variables, ϕ_{opt} and $\boldsymbol{\vartheta}$, are given. The two optimized design variables are not updated at all during the process here, and handled as fixed quantities rather than design variables in the optimization problem of producing fiber path lines described in Eqs. (43) to (46). Next, the objective functional is evaluated. When the objective functional has converged sufficiently to generate equally spaced and continuous fiber path lines, the optimization is terminated as an optimized configuration has been obtained. On the other hand, if it is considered that the calculations have not converged, the sensitivity to the scalar function ψ is calculated and the design variables are updated. The updating scheme is introduced in a later section. It then goes back to the step of solving the governing equations and evaluating the objective functional. Iterating the above procedure, we obtain the optimal scalar function ψ such that its contours are equally spaced and continuous path lines with no intersections.

4. Numerical examples

In Section 4.1, we show the validity and effectiveness of our proposed simultaneous optimization method via three numerical examples. First, we computed the stiffness maximization problem with isotropic material property for comparing our proposed method to a previous work [20]. Next, we take the orthotropic material into account and reproduce one example shown in Nomura et al. [16]. In this part, the validity of our proposed method is verified by identifying the optimal orientation and the direction of the principal stress under the single loading problem. In contrast to this simple problem, the optimal orientation cannot be predicted when multiple loadings are considered. We show the efficiency of our proposed method via the multi-loading problem. The common parameters for Section 4.1 are listed in Table 1. Each parameter has been introduced in Section 2.4. Otomori et al. [22] presented extensive numerical experiments to show the effect of these parameters.

In Section 4.2, we design the fiber path lines considering the manufacturability based on the obtained optimal orientation results. First, we demonstrate the superiority of our proposed method over the conventional commercial software algorithm. Second, we examine the effect of the initial guess on the path lines. The common parameters for Section 4.2 are listed in Table 2. These parameters play the same role as the level-set based topology optimization.

4.1. Stiffness maximization problem

4.1.1. Bridge structural problem

The fixed design domain D and the boundary conditions in this problem settings are shown in Fig. 7. The problem is nondimensionalized according to Eq. (5). The size of the fixed design domain D is 1×2. On the bottom boundary, the left part Γ_{u_0} is fixed, the right part Γ_{u_r} is roller supported, and the boundary load $\bar{\boldsymbol{t}} = [0, -5]^T$ is applied to the center part Γ_t. We set the isotropic material property as follows: $E_1 = E_2 = 1.0$, and $\mu_{12}(= \mu_{21}) = 0.31$ in Eqs. (10) and (11). The optimization problem can be described as follows,

$$\underset{\phi}{\text{minimize}} \quad \bar{F}[\phi] = \int_{\Gamma_t} \bar{\boldsymbol{t}} \cdot \boldsymbol{u} \mathrm{d}\Gamma + \frac{\tau_\phi}{2} \int_D \|\nabla\phi\|^2 \mathrm{d}D, \tag{51}$$

$$\text{subject to} \quad G[\phi] = \int_D \rho \mathrm{d}D - \bar{V} \leq 0, \tag{52}$$

$$\int_D \tilde{\boldsymbol{\sigma}} : \hat{\tilde{\boldsymbol{\varepsilon}}} \mathrm{d}D = \int_{\Gamma_t} \bar{\boldsymbol{t}} \cdot \hat{\boldsymbol{u}} \mathrm{d}\Gamma. \tag{53}$$

The maximum allowed volume is set to $\bar{V} = 0.80$, namely, 40% of the fixed design domain D.

The optimal configuration by the proposed method is shown in Fig. 8. We obtained the practically identical configuration with previous research by Yamada et al. [20], and confirmed that the topology optimization using the level set-based method introduced to this research has been performed adequately.

4.1.2. Cantilever beam problem

In order to show the validity of our proposed method, we present a numerical example of a cantilever beam problem and compare it with previous work [16]. This section considers the stiffness maximization problem for the single loading case under the volume constraint. The design settings are shown in Fig. 9, and the detail settings are as follows. The size of the fixed design region D is 1×2, the left side

Table 1
Common parameter settings of the stiffness maximization problems in Section 4.1.

Symbol	Value	Description
δ_ϕ	0.2	Transition width of the smoothed Heaviside function
d	1.0×10^{-5}	Ratio of Young's modulus between material and void domains
τ_ϕ	1.0×10^{-3}	Regularization coefficient of the level-set function ϕ
$\tau_{\boldsymbol{\vartheta}}$	1.0×10^{-3}	Regularization coefficient of double-angle direction vector $\boldsymbol{\vartheta}$
ϕ_{init}	0.5	Initial value of the level-set function ϕ
m_ϕ	0.25	Proportionality constant for the time derivative term of the level-set function ϕ
$m_{\boldsymbol{\vartheta}}$	1.5	Proportionality constant for the time derivative term of the double-angle direction vector $\boldsymbol{\vartheta}$
Λ_ϕ	1.0×10^{2}	Penalty coefficient of the level-set function ϕ
$\Lambda_{\boldsymbol{\vartheta}}$	1.0×10^{1}	Penalty coefficient of the double-angle direction vector $\boldsymbol{\vartheta}$
Δx	0.05	Mesh size of the finite elements in the numerical computations

Table 2
Common parameter settings of the optimization problem for generating fiber path lines in Section 4.2.

Symbol	Value	Description
C_{orth}	1.0	Coefficients determining the contribution of primary objective functional F_{orth}, Eq. (44)
C_{df}	0.2	Coefficients determining the contribution of primary objective functional F_{df}, Eq. (45)
τ_ψ	1.0×10^{-3}	Regularization coefficient of scalar function ψ, Eq. (46)
m_ψ	1.0	Proportionality constant for the time derivative term of scalar function ψ, Eq. (47)
Δx_1	0.05	Finite element mesh size for the first numerical computation
Δx_2	0.02	Finite element mesh size for the second numerical computation
$\Delta\psi$	1.5×10^{-2}	Parameter that determines the interval to display the contours of scalar function ψ
ψ_0	0	Value of point constraint to be imposed to scalar function ψ

Fig. 9. Design settings for case 1: the cantilever problem under a vertical load.

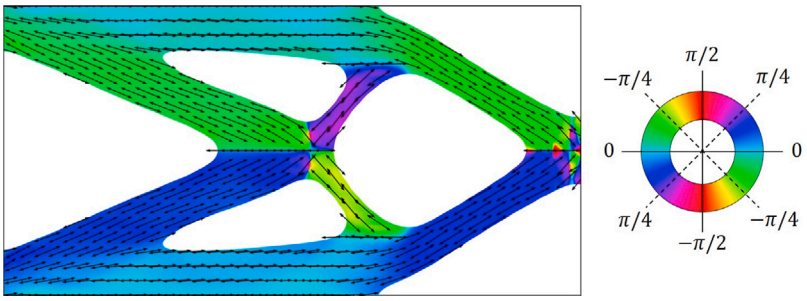

Fig. 10. Optimal configuration with color chart.

boundary Γ_{u_1} is fixed, and boundary load $\bar{\boldsymbol{t}}_1 = [0,-1]^T$ is applied to the center of the right side Γ_{t_1}. We set the orthotropic material property as follows: $E_1 = 1.0$, $E_2 = 0.1$ and $\mu_{12} = 0.3$, ($\nu_{21} = \nu_{12}E_2/E_1 = 0.03$). The initial value of the double angle-direction vector $\boldsymbol{\vartheta}$ is set to $[\varsigma_{\text{init}}(\boldsymbol{x}), \zeta_{\text{init}}(\boldsymbol{x})]^T = [0.25, 0.00]^T$. The optimization problem is described as follows:

$$\begin{aligned}\underset{\phi,\boldsymbol{\vartheta}}{\text{minimize}} \quad \bar{F}[\phi,\boldsymbol{\vartheta}] &= \int_{\Gamma_t} \bar{\boldsymbol{t}}_1\cdot\boldsymbol{u}\mathrm{d}\Gamma + \frac{\tau_\phi}{2}\int_D \|\nabla\phi\|^2\mathrm{d}D \\ &+ \frac{\tau_{\boldsymbol{\vartheta}}}{4}\int_D \{\nabla\boldsymbol{\vartheta}+(\nabla\boldsymbol{\vartheta})^{\mathrm{T}}\} : \{\nabla\boldsymbol{\vartheta}+(\nabla\boldsymbol{\vartheta})^{\mathrm{T}}\}\mathrm{d}D, \end{aligned} \tag{54}$$

$$\text{subject to} \quad G[\phi] = \int_D \rho\mathrm{d}D - \bar{V} \le 0 \tag{55}$$

$$\int_D \tilde{\boldsymbol{\sigma}} : \hat{\boldsymbol{\varepsilon}}\mathrm{d}D = \int_{\Gamma_t} \bar{\boldsymbol{t}}_1\cdot\hat{\boldsymbol{u}}\mathrm{d}\Gamma. \tag{56}$$

We set the upper volume constraint as 50% of the fixed design domain D, i.e., $\bar{V} = 1.0$.

The optimal result by the proposed method is shown in Fig. 10. The color chart represents the direction angle in the range $[-\pi/2, \pi/2]$, and the arrows clearly indicate the orientation at each point. Comparing our result to that of the previous research by Nomura et al. [16], it can

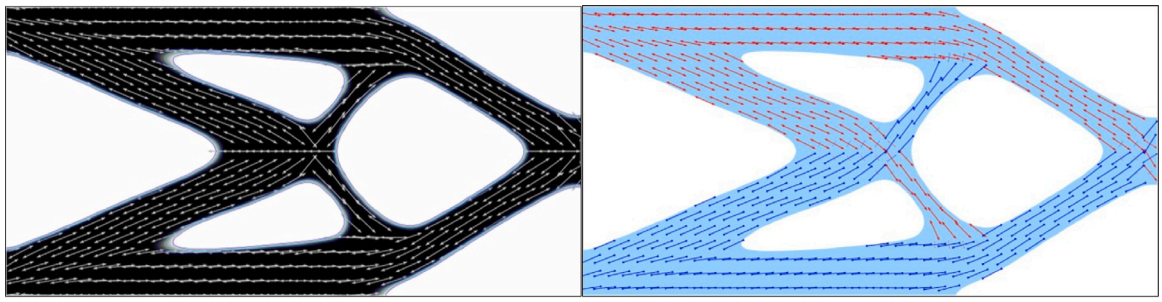

(a) Optimal configuration (b) Direction of the principal stress

Fig. 11. Comparison between (a) optimal configuration and (b) the direction of the principal stress in case 1.

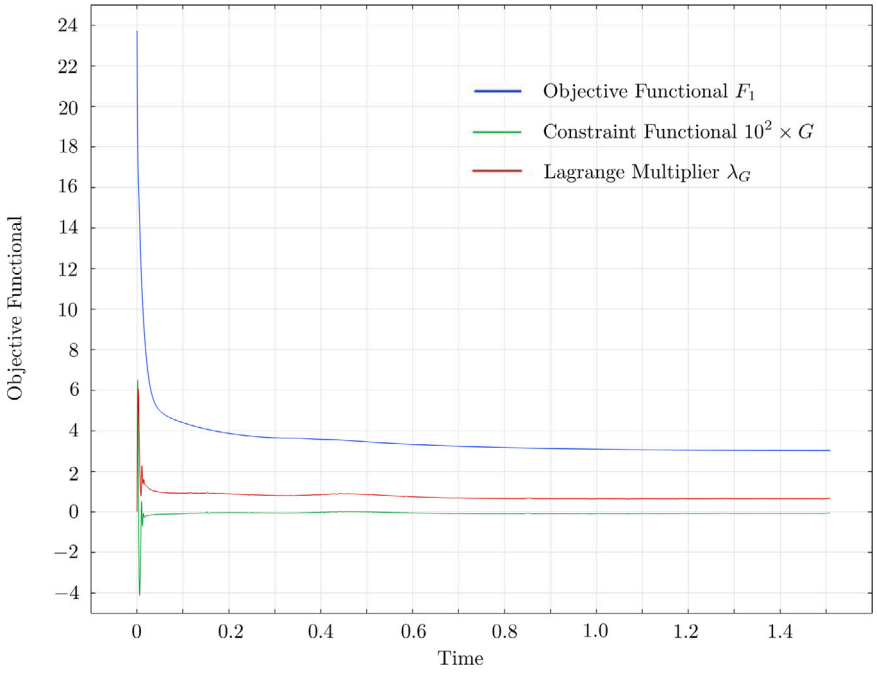

Fig. 12. Convergence history for optimization of case 1: objective functional F_1 (Eq. (29)), constraint functional $10^2 \times G$ (Eq. (32)) and Lagrange multiplier λ_G (Eq. (35)).

be said that the structural configurations and orientations are almost identical.

The optimal configuration and the distribution of the normalized principal stress are shown in Fig. 11 and the convergence history of the optimization is shown in Fig. 12. From these results, it can be said that the distribution of orientation and the normalized principal stresses are in pretty good agreement, and that a design solution with high stiffness has been achieved. For brevity herein after, we name this single-loading problem as case 1 and the optimal solution (Fig. 11(a)) as S_1.

We consider the other design settings as case 2, which is shown in Fig. 13. The boundary load to the center of right boundary Γ_{t_2} is $\bar{\boldsymbol{t}}_2 = [2, 0]^T$. The objective functional is defined as follows,

$$\underset{\phi,\boldsymbol{\vartheta}}{\text{minimize}} \quad \bar{F}[\phi,\boldsymbol{\vartheta}] = \int_{\Gamma_t} \bar{\boldsymbol{t}}_2 \cdot \boldsymbol{u}\mathrm{d}\Gamma + \frac{\tau_\phi}{2}\int_D \|\nabla\phi\|^2\mathrm{d}D + \frac{\tau_{\boldsymbol{\vartheta}}}{4}\int_D \{\nabla\boldsymbol{\vartheta} + (\nabla\boldsymbol{\vartheta})^{\mathrm{T}}\} : \{\nabla\boldsymbol{\vartheta} + (\nabla\boldsymbol{\vartheta})^{\mathrm{T}}\}\mathrm{d}D. \tag{57}$$

The other settings are identical with case 1.

The obtained optimal configuration and the distribution of the normalized principal stresses are presented in Fig. 14, and the convergence history of the optimization is plotted in Fig. 15. We obtained the well-known optimal configuration and also obtained the reasonable orientation angle, which identified with the direction of the principal stress. This optimal solution (Fig. 14(a)) is named as S_2.

4.1.3. Multi-loading problem

The optimal orientation does not identify with the principal stress direction and the orientation cannot be predicted in multi-loading problem. So, this section shows the efficiency of our proposed method by applying it to the multi-loading problem combining cases 1 and 2 in Section 4.1.2. The optimization problem is defined as follows:

$$\underset{\phi,\boldsymbol{\vartheta}}{\text{minimize}} \quad \bar{F}[\phi,\boldsymbol{\vartheta}] = \max\left(\int_{\Gamma_t} \bar{\boldsymbol{t}}_1 \cdot \boldsymbol{u}_1\mathrm{d}\Gamma,\ \int_{\Gamma_t} \bar{\boldsymbol{t}}_2 \cdot \boldsymbol{u}_2\mathrm{d}\Gamma\right) + \frac{\tau_\phi}{2}\int_D \|\nabla\phi\|^2\mathrm{d}D + \frac{\tau_{\boldsymbol{\vartheta}}}{4}\int_D \{\nabla\boldsymbol{\vartheta} + (\nabla\boldsymbol{\vartheta})^{\mathrm{T}}\} : \{\nabla\boldsymbol{\vartheta} + (\nabla\boldsymbol{\vartheta})^{\mathrm{T}}\}\mathrm{d}D, \tag{58}$$

$$\text{subject to} \quad G[\phi] = \int_D \rho\mathrm{d}D - \bar{V} \le 0 \tag{59}$$

$$\int_D \tilde{\boldsymbol{\sigma}}_1 : \hat{\tilde{\boldsymbol{\varepsilon}}}_1\mathrm{d}D = \int_{\Gamma_t} \bar{\boldsymbol{t}}_1 \cdot \hat{\boldsymbol{u}}_1\mathrm{d}\Gamma. \tag{60}$$

$$\int_D \tilde{\boldsymbol{\sigma}}_2 : \hat{\tilde{\boldsymbol{\varepsilon}}}_2\mathrm{d}D = \int_{\Gamma_t} \bar{\boldsymbol{t}}_2 \cdot \hat{\boldsymbol{u}}_2\mathrm{d}\Gamma. \tag{61}$$

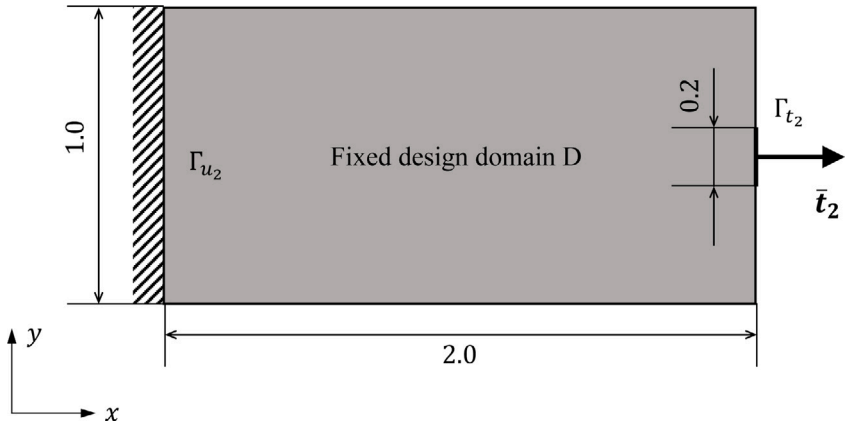

Fig. 13. Design settings for case 2: the cantilever problem under a horizontal load.

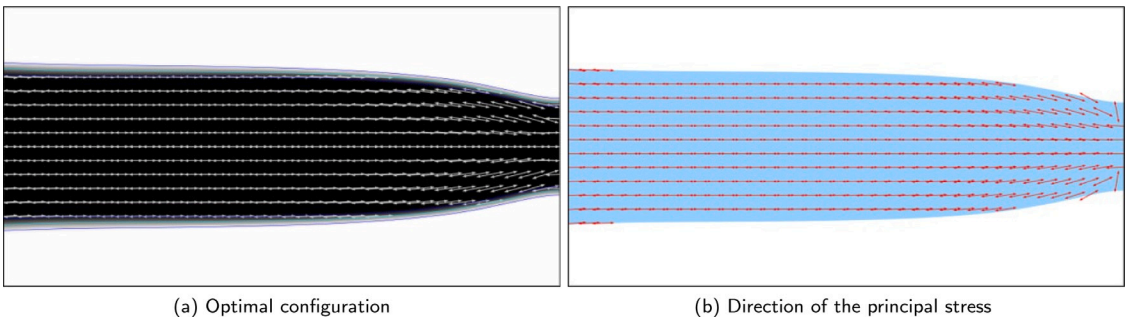

Fig. 14. Comparison between (a) optimal configuration and (b) the direction of the principal stress in case 1.

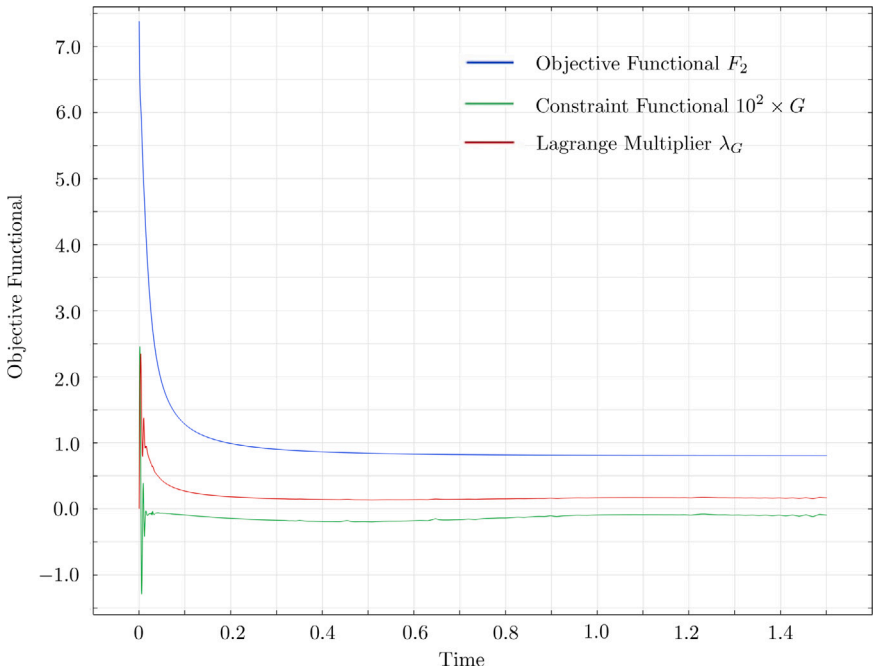

Fig. 15. Convergence history for optimization of case 2: objective functional F_2 (Eq. (29)), constraint functional $10^2 \times G$ (Eq. (32)) and Lagrange multiplier λ_G (Eq. (35)).

Here, to regularize the optimization problem, the objective functionals F_1 and F_2 in Eq. (28) were normalized by the terminated objective values, $F_{1_{\text{opt}}} = 3.026$ and $F_{2_{\text{opt}}} = 0.807$, respectively.

The obtained optimal result, the normalized principal stress distribution, and the convergence history of the optimization are shown in Figs. 16–18, respectively. The distribution of directions in the optimal solution is different from the directions in cases 1 and 2. The convergence history confirms that the objective functionals F_1 and F_2 are stable enough to converge, and that the numerical computation has been properly performed. As with the results in Section 4.1.2, the optimal solution (Fig. 16) is named as M. We perform the crosscheck, that is, the optimal results, S_1, S_2, and M, are evaluated via each

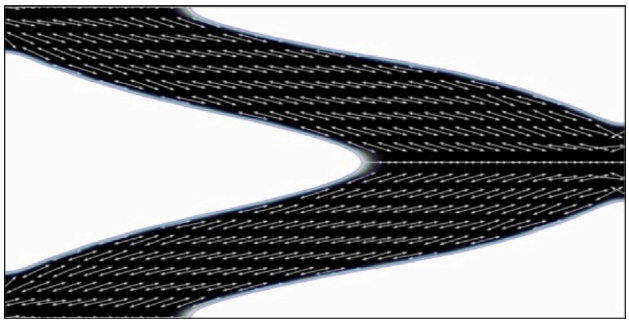

Fig. 16. Optimal configuration for the multi-loading problem.

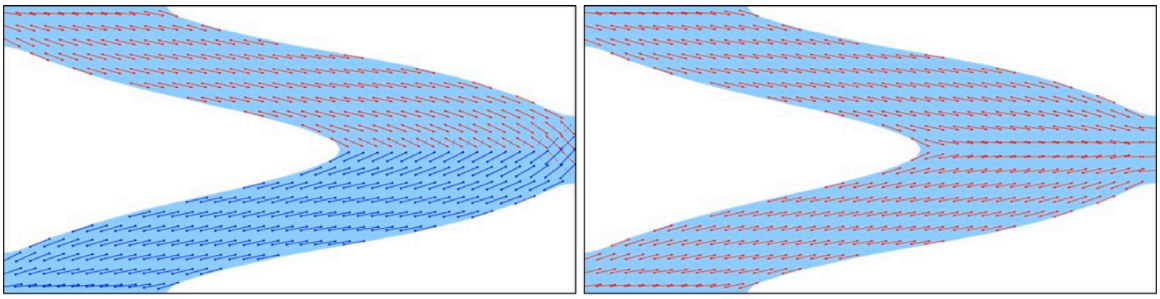

Fig. 17. Direction of the principal stress for the multi-loading problem.

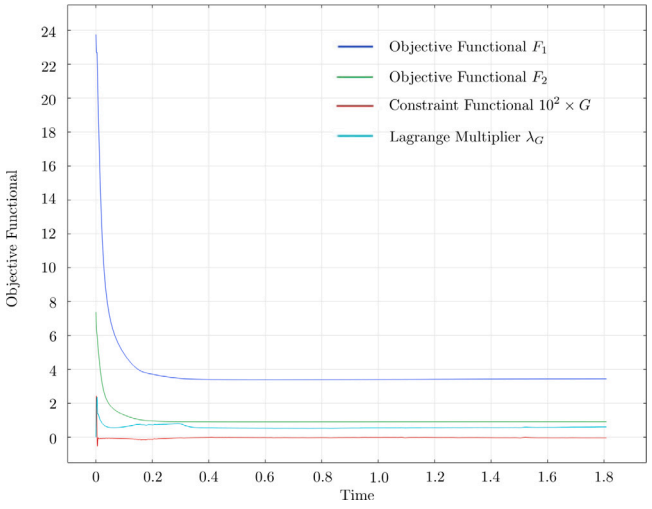

Fig. 18. Iterative histories for multi-loading case: objective functional F_1, F_2 (Eq. (29)), constraint functional $10^2 \times G$ (Eq. (32)) and Lagrange multiplier λ_G (Eq. (35)).

terminated objective value in Table 3. The minimum values of F_1 and F_2 are obtained in S_1 and S_2, respectively. And, S_1 has the worst value for case 2, and S_2 vice versa. On the other hand, the optimal result, M, has enough small values for both the objective functional values F_1 and F_2.

As these numerical examples show, we successfully computed our simultaneous optimization algorithm even in the complicated multi-loading problem.

Table 3
Crosscheck for the objective values.

Case	F_1 (vs. vertical loading)	F_2 (vs. horizontal loading)
Configuration S_1	3.026(minimum value)	2.235(+177.0%)
Configuration S_2	10.765(+255.8%)	0.807(minimum value)
Configuration M	3.448(+13.9%)	0.916(+13.5%)

4.2. Optimization problem of generating fiber path lines

This section shows the validity of our proposed method for generating fiber path lines. The left center of the fixed design domain D is set as the origin $\boldsymbol{x}_0 = [0, 0]^{\mathrm{T}}$ of the coordinate system, and a point constraint $\psi(\boldsymbol{x}_0) = \psi_0$ with a scalar function ψ is imposed at $\boldsymbol{x}_0$. The initial distribution ψ_{init} of the scalar function ψ is given, and optimization is carried out with the finite element mesh size Δx_1 until numerical calculations converge. Then, its converged solution is set as the initial value, and the optimization is performed again with the finite element mesh size Δx_2, which is smaller than Δx_1. Finally, the terminated scalar function ψ is regarded as the optimal solution ψ_{opt}, and its contour line represents the fiber path lines.

We generated the fiber path lines for the three optimal results, S_1, S_2 and M. The initial distribution of the scalar function ψ is set as $\psi_{\mathrm{init}}(\boldsymbol{x}) = |y|$. In order to show the effectiveness of our proposed method, the design of fiber path lines generated by our proposed method was compared to the streamlines automatically generated by COMSOL Multiphysics for S_1, S_2, and M in Figs. 19–21. In these examples, the fiber path lines made by the proposed method were aligned along a given direction. Comparing (a) and (b), it can be concluded that our constructed method is more capable of arranging fibers with guaranteed equal spacing and continuity than the streamline

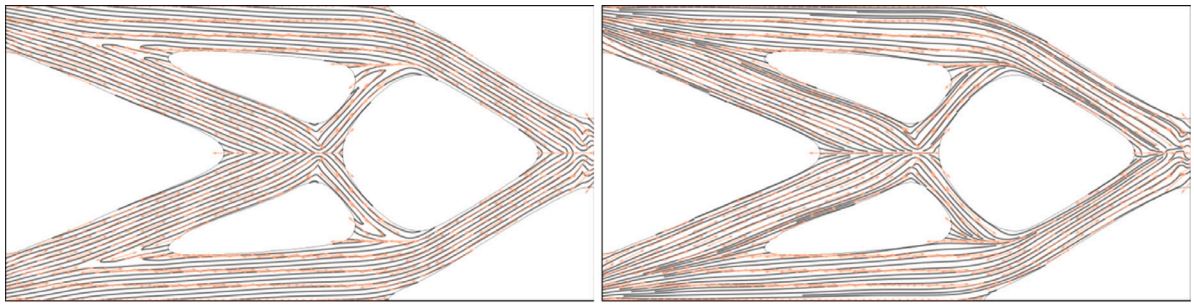

(a) Fiber path lines generated by optimization: ψ contours. (b) Automatically generated streamlines.

Fig. 19. Comparison between (a) the proposed method and (b) algorithm of commercial software for the single vertical loading problem.

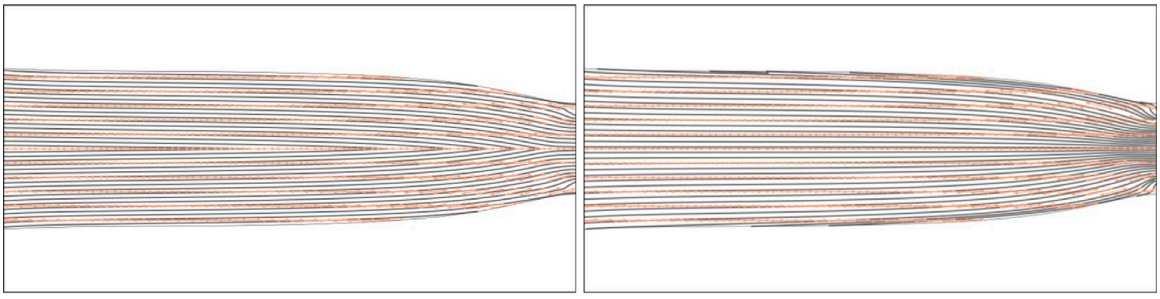

(a) Fiber path lines generated by optimization: ψ contours. (b) Automatically generated streamlines.

Fig. 20. Comparison between (a) the proposed method and (b) algorithm of commercial software for the single horizontal loading problem.

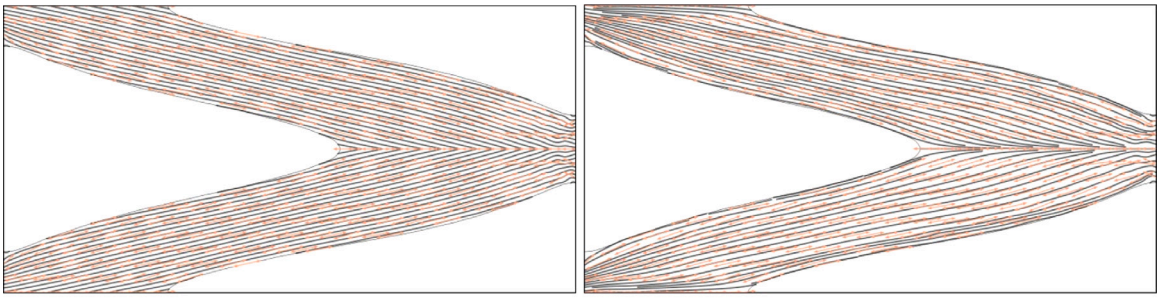

(a) Fiber path lines generated by optimization: ψ contours. (b) Automatically generated streamlines.

Fig. 21. Comparison between (a) the proposed method and (b) algorithm of commercial software for the multi-loading problem.

Table 4
Comparison of the objective functional values.

Case	Stiffness maximization only	After fiber arrangement
Configuration S_1	$F_1 = 3.026$	$F_1 = 3.108(+2.71\%)$
Configuration S_2	$F_2 = 0.807$	$F_2 = 0.817(+1.24\%)$
Configuration M	$F_1 = 3.448 F_2 = 0.916$	$F_1 = 3.512\,(+1.86\%) F_2 = 0.937\,(+2.29\%)$

based results. The values of upsampled results were compared with the results before being interpreted in Table 4. From the table, it can be observed that the values of F_1 and F_2 before and after being interpreted were quite close to each other with the maximum discrepancy of 2.71%. On the other hand, the generated fiber path lines were almost equally spaced and continuous.

Next, we ran the same algorithm for the optimal result, M, as input, but using different initial distribution of the scalar function, ψ, as following three cases, $\psi_{\text{init}}(\boldsymbol{x}) = \sqrt{x^2 + y^2}$, x and $(-|x| + |y|)/\sqrt{2}$.

The results are shown in Fig. 22. The path lines of the fibers inside the structure have a similar pattern for any initial distribution ψ_{init} of the scalar function ψ, which are equally spaced and continuous.

Through the above numerical examples in Section 4.2, we concluded that our proposed method is capable of generating fiber path lines with good manufacturability.

5. Conclusions

In the design of continuous fiber materials, ensuring an even and continuous distribution of fibers is critical. Here, we propose an integrated two-step approach for topology optimization and fiber arrangement in continuous-fiber composites.

In the first phase, we formulated the structural shape and orientation design problem with the objective of maximizing stiffness. To

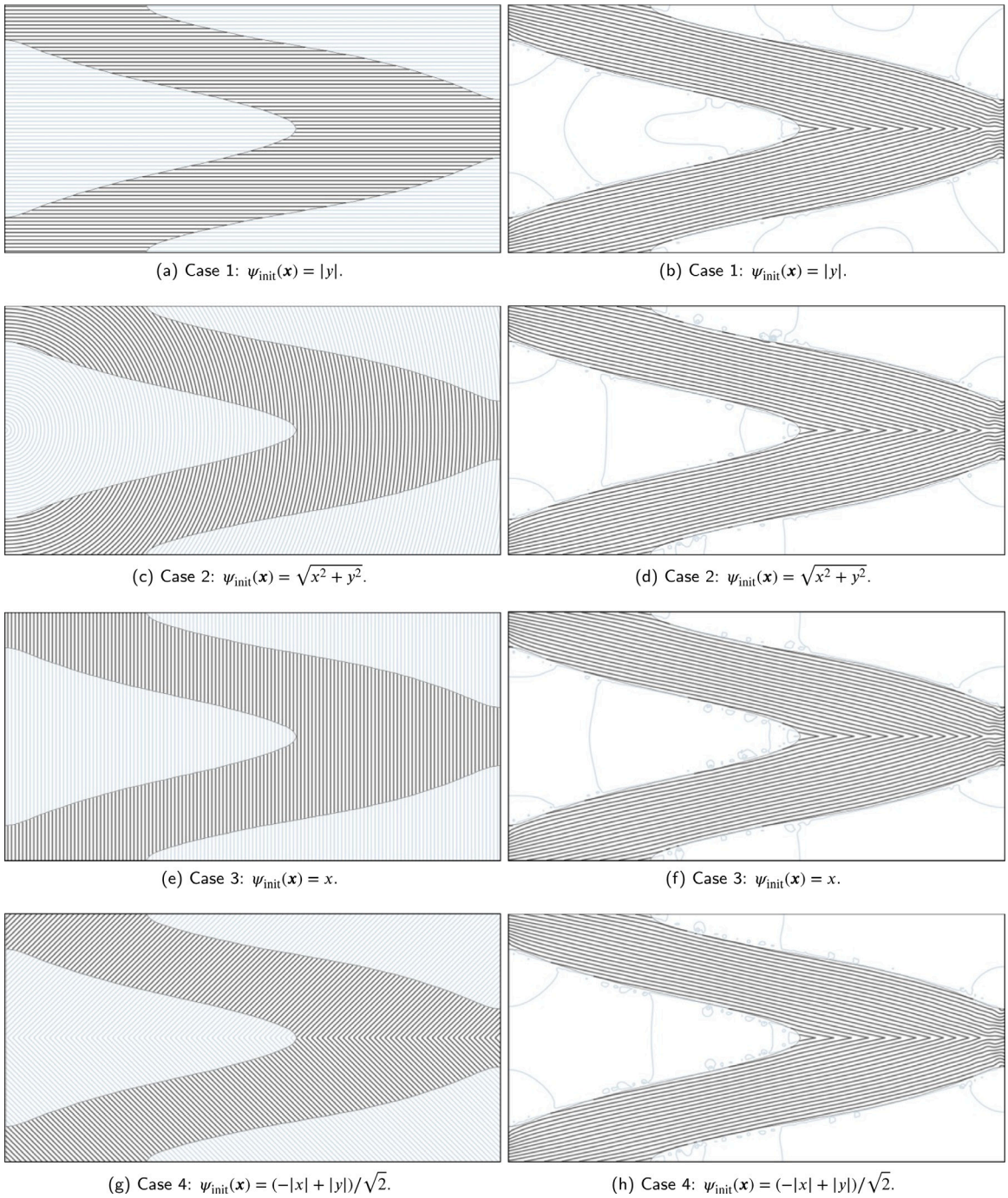

(a) Case 1: $\psi_{\text{init}}(\boldsymbol{x}) = |y|$. (b) Case 1: $\psi_{\text{init}}(\boldsymbol{x}) = |y|$.

(c) Case 2: $\psi_{\text{init}}(\boldsymbol{x}) = \sqrt{x^2 + y^2}$. (d) Case 2: $\psi_{\text{init}}(\boldsymbol{x}) = \sqrt{x^2 + y^2}$.

(e) Case 3: $\psi_{\text{init}}(\boldsymbol{x}) = x$. (f) Case 3: $\psi_{\text{init}}(\boldsymbol{x}) = x$.

(g) Case 4: $\psi_{\text{init}}(\boldsymbol{x}) = (-|x| + |y|)/\sqrt{2}$. (h) Case 4: $\psi_{\text{init}}(\boldsymbol{x}) = (-|x| + |y|)/\sqrt{2}$.

Fig. 22. Optimal configurations obtained by using different initial guesses: initial configuration (left) and optimal configuration (right).

achieve this, we employed a level set-based topology optimization method for topological design, which resulted in clear boundaries without grayscale. For angle design, we introduced a novel design variable known as the "double angle vector" denoted as $\boldsymbol{\vartheta}$, which significantly improved optimization by reducing the likelihood of converging to a local optimum. Furthermore, we derived design sensitivities for the concurrent optimization method and utilized reaction–diffusion equations to update the design variables, ϕ and $\boldsymbol{\vartheta}$.

Continuous fiber materials must be manufactured with continuous and equal spacing between them. In the second phase, we proposed an optimization problem to obtain manufacturable fiber paths based on the results from the first stage. We introduced a scalar function, denoted as ψ, as a design variable and optimized it in a way that its contours align with the optimal orientation angles. We also derived the design sensitivity for drawing the path lines and employed reaction–diffusion equations to update the design variable, ψ. This consistent updating scheme shared with the first stage offers advantages in terms of ease of implementation and parameter studies.

We conducted numerical examples to show the validity and efficiency of our proposed optimal design method. In Sections 4.1.1 and 4.1.2, we demonstrated the validity of our concurrent optimization method by comparing it to two conventional methods. The first example addressed the isotropic material problem, while the second example pertained to anisotropic material, where we observed the alignment of the optimum orientation results with the direction of the principal stress, consistent with prior research. In Section 4.1.3, we tackled

an optimization problem for a multi-loading case to demonstrate the efficiency of our proposed method. We successfully obtained optimal results that were not contingent on the principal stress directions. The second phase of our method was employed to generate manufacturable fiber path lines in Section 4.2. Based on the results of Sections 4.1.2 and 4.1.3, we successfully achieved even and continuous distribution of the fiber path lines. Furthermore, we confirmed reduced dependency on initial configurations compared to previous methods. Finally, through the numerical examples, we demonstrated that our proposed method efficiently achieves optimal designs considering the manufacturability of continuous fibers.

CRediT authorship contribution statement

Yusuke Fujimoto: Methodology, Software, Validation, Writing – original draft. **Kozo Furuta:** Methodology, Writing – review & editing, Funding acquisition. **Tsuguo Kondoh:** Conceptualization, Methodology, Software, Writing – review & editing. **Hao Li:** Methodology, Writing – review & editing. **Kazuhiro Izui:** Conceptualization, Supervision, Writing – review & editing. **Shinji Nishiwaki:** Conceptualization, Supervision, Writing – review & editing, Funding acquisition.

Declaration of competing interest

The authors declare that they have no competing financial interests for this paper.

Data availability

Data will be made available on request.

Acknowledgments

This paper is based on results obtained from a project, JPNP14005, subsidized by the New Energy and Industrial Technology Development Organization (NEDO), Japan and supported by JSPS, Japan KAKENHI Grant Number 22K14168.

References

[1] Nabil F. Grace, G.A. Sayed, A.K. Soliman, K.R. Saleh, Strengthening reinforced concrete beams using fiber reinforced polymer (FRP) laminates, ACI Struct. J.-Am. Concrete Inst. 96 (5) (1999) 865–874.
[2] Chun-Hway Hsueh, Young's modulus of unidirectional discontinuous-fibre composites, Compos. Sci. Technol. 60 (14) (2000) 2671–2680.
[3] Peter J. Hine, Hans Rudolf Lusti, Andrei A. Gusev, Numerical simulation of the effects of volume fraction, aspect ratio and fibre length distribution on the elastic and thermoelastic properties of short fibre composites, Compos. Sci. Technol. 62 (10–11) (2002) 1445–1453.
[4] Pierre Debout, Helene Chanal, Emmanuel Duc, Tool path smoothing of a redundant machine: Application to automated fiber placement, Comput. Aided Des. 43 (2) (2011) 122–132.
[5] Ermias G Koricho, Anton Khomenko, Tommy Fristedt, Mahmoodul Haq, Innovative tailored fiber placement technique for enhanced damage resistance in notched composite laminate, Compos. Struct. 120 (2015) 378–385.
[6] Martin Philip Bendsøe, Noboru Kikuchi, Generating optimal topologies in structural design using a homogenization method, Comput. Methods Appl. Mech. Engrg. 71 (2) (1988) 197–224.
[7] Michael Bruyneel, Claude Fleury, Composite structures optimization using sequential convex programming, Adv. Eng. Softw. 33 (7–10) (2002) 697–711.
[8] Esben Lindgaard, Erik Lund, Optimization formulations for the maximum nonlinear buckling load of composite structures, Struct. Multidiscip. Optim. 43 (5) (2011) 631–646.
[9] Anthony Garland, Georges Fadel, Optimizing topology and gradient orthotropic material properties under multiple loads, J. Comput. Inf. Sci. Eng. 19 (2) (2019).
[10] Jan Stegmann, Erik Lund, Discrete material optimization of general composite shell structures, Internat. J. Numer. Methods Engrg. 62 (14) (2005) 2009–2027.
[11] Yuqing Zhou, Tsuyoshi Nomura, Kazuhiro Saitou, Multi-component topology and material orientation design of composite structures (MTO-C), Comput. Methods Appl. Mech. Engrg. 342 (2018) 438–457.
[12] Yunfeng Luo, Wenjiong Chen, Shutian Liu, Quhao Li, Yaohui Ma, A discrete-continuous parameterization (DCP) for concurrent optimization of structural topologies and continuous material orientations, Compos. Struct. 236 (2020) 111900.
[13] José Pedro Blasques, Multi-material topology optimization of laminated composite beams with eigenfrequency constraints, Compos. Struct. 111 (2014) 45–55.
[14] Christopher J. Brampton, K. Chauncey Wu, H. Alicia Kim, New optimization method for steered fiber composites using the level set method, Struct. Multidiscip. Optim. 52 (3) (2015) 493–505.
[15] Hang Li, Liang Gao, Hao Li, Xiaopeng Li, Haifeng Tong, Full-scale topology optimization for fiber-reinforced structures with continuous fiber paths, Comput. Methods Appl. Mech. Engrg. 377 (2021) 113668.
[16] Tsuyoshi Nomura, Ercan M Dede, Jaewook Lee, Shintaro Yamasaki, Tadayoshi Matsumori, Atsushi Kawamoto, Noboru Kikuchi, General topology optimization method with continuous and discrete orientation design using isoparametric projection, Internat. J. Numer. Methods Engrg. 101 (8) (2015) 571–605.
[17] Tsuyoshi Nomura, Atsushi Kawamoto, Tsuguo Kondoh, Ercan M Dede, Jaewook Lee, Yuyang Song, Noboru Kikuchi, Inverse design of structure and fiber orientation by means of topology optimization with tensor field variables, Composites B 176 (2019) 107187.
[18] Yuqing Zhou, Tsuyoshi Nomura, Kazuhiro Saitou, Anisotropic multicomponent topology optimization for additive manufacturing with build orientation design and stress-constrained interfaces, J. Comput. Inf. Sci. Eng. 21 (1) (2021).
[19] Jeroen P. Groen, Ole Sigmund, Homogenization-based topology optimization for high-resolution manufacturable microstructures, Internat. J. Numer. Methods Engrg. 113 (8) (2018) 1148–1163, http://dx.doi.org/10.1002/nme.5575, arXiv:https://onlinelibrary.wiley.com/doi/pdf/10.1002/nme.5575. URL https://onlinelibrary.wiley.com/doi/abs/10.1002/nme.5575.
[20] Takayuki Yamada, Kazuhiro Izui, Shinji Nishiwaki, Akihiro Takezawa, A topology optimization method based on the level set method incorporating a fictitious interface energy, Comput. Methods Appl. Mech. Engrg. 199 (45–48) (2010) 2876–2891.
[21] Jan Stegmann, Analysis and Optimization of Laminated Composite Shell Structures (Ph.D. thesis), Instituite of Mechanical Engineering, Aalborg University, Denmark, 2004.
[22] Masaki Otomori, Takayuki Yamada, Kazuhiro Izui, Shinji Nishiwaki, Matlab code for a level set-based topology optimization method using a reaction diffusion equation, Struct. Multidiscip. Optim. 51 (2015) 1159–1172.